Fiber Optic Vacuum Ultraviolet Sensor Based on an AlN-Microwire Probe

Ying WANG[1,2*], Jiahui YE[1,2], Dingbang MA[1,2], Peiyao WANG[1], Baikui LI[1], Zhenhua SUN[1], Honglei WU[1*], Changrui LIAO[1,2], and Yiping WANG[1,2]

[1]*Shenzhen Key Laboratory of Ultrafast Laser Micro/Nano Manufacturing, Key Laboratory of Optoelectronic Devices and Systems of Ministry of Education/Guangdong Province, College of Physics and Optoelectronic Engineering, Shenzhen University, Shenzhen 518060, China*

[2]*Shenzhen Key Laboratory of Photonic Devices and Sensing Systems for Internet of Things, Guangdong and Hong Kong Joint Research Centre for Optical Fibre Sensors, State Key Laboratory of Radio Frequency Heterogeneous Integration, Shenzhen University, Shenzhen 518060, China*

[*]Corresponding authors: Ying WANG and Honglei WU E-mails: yingwang@szu.edu.cn and hlwu@szu.edu.cn

Abstract: Vacuum ultraviolet (VUV) light sensing shows great potential applications in the space science, materials, biophysics, and plasma physics. In this work, an all-optical detection method is proposed for VUV sensing by constructing an optical fiber-end Fabry-Pérot interferometer based on a single aluminum nitride (AlN) microwire. Compared with the traditional electrical devices, this all-optical detection method overcomes the difficulties like the fast response and electromagnetic interference immunity in detecting VUV bands at the present stage, and improves the response speed. The proposed device shows the excellent performance of VUV detection, with the static sensitivity of 1.03 nm/(W·cm^{-2}), response rise time of down to 10 μs, and decay time of 0.64 ms. Beneficial from the excellent radiation resistance of AlN microwires and UV resistance of silica fibers, the proposed device is expected to have the good stability and potential applications in the fields of the solar physics and space exploration.

Keywords: Optical fiber sensor; VUV; Fabry-Pérot interferometer; UV sensing

Citation: Ying WANG, Jiahui YE, Dingbang MA, Peiyao WANG, Baikui LI, Zhenhua SUN, *et al*., "Fiber Optic Vacuum Ultraviolet Sensor Based on an AlN-Microwire Probe," *Photonic Sensors*, 2025, 15(1): 250117.

1. Introduction

Vacuum ultraviolet (VUV) sensing is of great significance in the fields of the solar physics, space science, semiconductor industry, and biopharmaceutical and basic science [1–10]. For example, due to the fact of significant differences in the VUV region of the solar spectrum during intense solar activities, the VUV sensing technology is considered to be an extremely effective method to monitor the solar wind, track the evolution of stars, and predict the space weather [11, 12]. In the field of the semiconductor industry, the high-performance VUV sensing technology is also very important for high-resolution lithography such as 193 nm and 157 nm excimer laser lithography and 13.5 nm extreme ultraviolet (EUV) lithography, where the VUV sensing technology with the excellent

Received: 27 October 2023 / Revised: 31 January 2024

DOI: 10.1007/s13320-024-0728-y
Article type: Regular

performance is needed to monitor the single pulse energy with the high accuracy in real time [13]. In basic sciences, VUV is widely used in the fields of high-energy physics, nonlinear optics, spectroscopy, surface physics, photochemistry, and so on [14]. The inherent requirements of this cutting-edge science have become an important driving force for the development of the high-performance VUV sensing technology.

The VUV light-band spans from 10 nm to 200 nm, which will be strongly absorbed by atoms and molecules of oxygen in the air and can only propagate in vacuum [15]. Limited by the propagation environment and the lack of VUV-related devices and technologies, the VUV sensing technology is still difficult to be widely studied. Critical requirements inspired by extreme environment applications further pose special physical and technical challenges to VUV sensing; for example, the VUV sensor should exhibit high radiation hardness (i.e., no apparent degradation in the presence of high-energy particle radiation), a low noise level, and a high signal-to-noise ratio (SNR) to realize weak signal detection, besides the requirement of the clean and high vacuum working environment [16]. In order to meet these challenges, many types of VUV sensing schemes have been investigated, such as the scintillator, photomultiplier, gas sensing, and semiconductor photodetector [17–21]. The scintillator visualizes the invisible VUV light through the optical down-conversion process and then realizes the VUV sensing combined with the "visible" band light detector or ultrafast camera, of which the system is commonly bulky and complex [17]. The VUV photomultiplier shows the ultra-high sensitivity and ultra-low noise through the external photoelectric effect and photoelectron multiplication process, which has become an excellent device for weak VUV signal sensing [18]. However, the performance of the device depends heavily on window materials (namely, the optical filter) and is not suitable for intense light operation [19]. The gas sensing technology takes gas as the working medium, producing plasmas and outputting electrical signals on the electrode after being irradiated by VUV light, which shows the high stability and long service life [20]. However, it generally only meets the demand of ultra-high power VUV radiation, the working voltage is very high, and the weight and volume are huge. To date, VUV sensing using the internal photoelectric effect of semiconductors, especially the ultra-wide band-gap (UWBG) semiconductor, is an emerging technology with attractive prospects [21]. The energy of 200 nm VUV photons (~6.2 eV) is close to the band-gap of some UWBG semiconductors [such as the aluminum nitride (AlN), BN, and diamond], thus UWBG semiconductors are excellent candidates for developing filterless VUV sensors. Besides the inherent excellent radiation hardness, they also exhibit the advantages of miniaturization and flexibility of integration.

The AlN is one of the important UWBG semiconductors, which exhibits the large direct band-gap (6.28 eV), high physical and chemical stability, high thermal conductivity, low thermal expansion, and excellent radiation hardness. Recently, the low-dimensional single-crystal AlN has been proven to be an ideal material for VUV sensing. For example, W. Zheng *et al.* [22] reported a VUV sensitive photodetector based on a high-quality single-crystal AlN micro/nanowire, with the response time of 0.1 s for 193 nm ultraviolet (UV) radiation. T. T. Li *et al.* [23] reported an AlN single-crystal film with the low defect density for VUV sensing, which exhibited the response time of 2.8 μs and decay time of 0.77 ms for 185 nm UV radiation. Up to now, the design of AlN VUV sensors generally employs the mechanism of the photovoltaic effect, photoconductivity gain, or avalanche ionization caused by the photo-generated carriers. However, the carrier mobility and high resistance always limit the sensing performance of the device on the time scale. Meanwhile, the metal

electrodes are prone to damage and reduce the device life under long-term VUV exposure. To solve these problems, here we propose an AlN-microwire based fiber optic device for fast and efficient VUV sensing, where the optical refractive index (RI) of the AlN microwire that changes transiently with the generation of photo-generated carriers is employed for the sensor design to improve the device response time and avoid the VUV damage to the external circuit [24]. For the realization of the proposed fiber optic sensor, an AlN microwire with a length of 210 μm and a diameter of 5 μm is integrated on the end-facet of a single mode fiber. Two end-facets of the AlN microwire can reflect the monitoring light delivered from the fiber core and form a fiber-tip Fabry-Pérot interferometer (FPI). Under VUV radiation, photo-generated carriers modify the RI of the AlN microwire as well as the optical path length of the FP interferometer, which will result in the inference wavelength shift on the device reflection spectrum. Experimental results show that the proposed fiber optic VUV sensor achieves the sensitivity of 1.033 nm/(W·cm^{-2}), response time of 10 μs, and decay time of 0.64 ms, respectively. Compared to that of the traditional VUV sensing technology, the proposed sensor exhibits the advantage of fast response, filter independence, miniaturization, light weight, and flexibility of deployment (benefitting from the flexible fiber optical path), which provides the great convenience for practical applications in many fields such as cosmology, astrophysics, high energy physics, semiconductor industry, and spectroscopy.

2. Materials and device fabrication

2.1 Preparation and characterization of AlN microwires

AlN microwires are prepared by the physical vapor transport method through necessary high-temperature growth and annealing processes. Figure 1(a) shows the typical scanning electron microscopy (SEM) image of a single AlN microwire with a hexagonal structure. The X-ray diffraction (XRD) result is shown in Fig. 1(b), which is in high consistency compared to that of the standard AlN card, indicating that there are no apparent impurities induced in the synthesis process. The main diffraction peak of the XRD pattern corresponds to the (101) plane of the AlN microwire, and the narrow full-width at half-maximum of all the diffraction orders confirms that the obtained AlN microwire has the good crystal quality. Note that the peaks corresponding to polycrystals in Fig. 1(b) are originated from the testing method that employs a lot of microwires. Figure 1(c) depicts the high-resolution transmission electron microscopy (TEM) image of the AlN microwire, where the spacing distance between the (0001) and (0002) planes can be measured to be 0.493 nm and 0.239 nm, respectively, indicating the good crystallinity and growth direction along the (0001) direction of the synthesized AlN microwires. Note that the upper-right inset is the selected-area electron diffraction (SAED) pattern, which also proves that the AlN microwire is the single crystal, and the calculated inter-planar spacing is the same as that obtained from the TEM image. Energy-dispersive X-ray (EDX) analysis is further used to examine the elemental composition of AlN microwires and the results are shown in Figs. 1(d) and 1(e), respectively, where the distribution of N and Al can be seen clearly. Figure 1(f) shows the Raman spectrum of the synthesized AlN microwire, where 6 phonon modes of A_1(TO), A_1(LO), E_1(TO), E_1(LO), E_{21}, and E_{22} can be observed clearly at 623 cm^{-1}, 891 cm^{-1}, 669 cm^{-1}, 909 cm^{-1}, 247 cm^{-1}, and 656 cm^{-1}, respectively, which further indicates that the AlN microwire has a hexagonal wurtzite crystal structure. The abovementioned results confirm that the synthesized material is high-quality single-crystal AlN microwires.

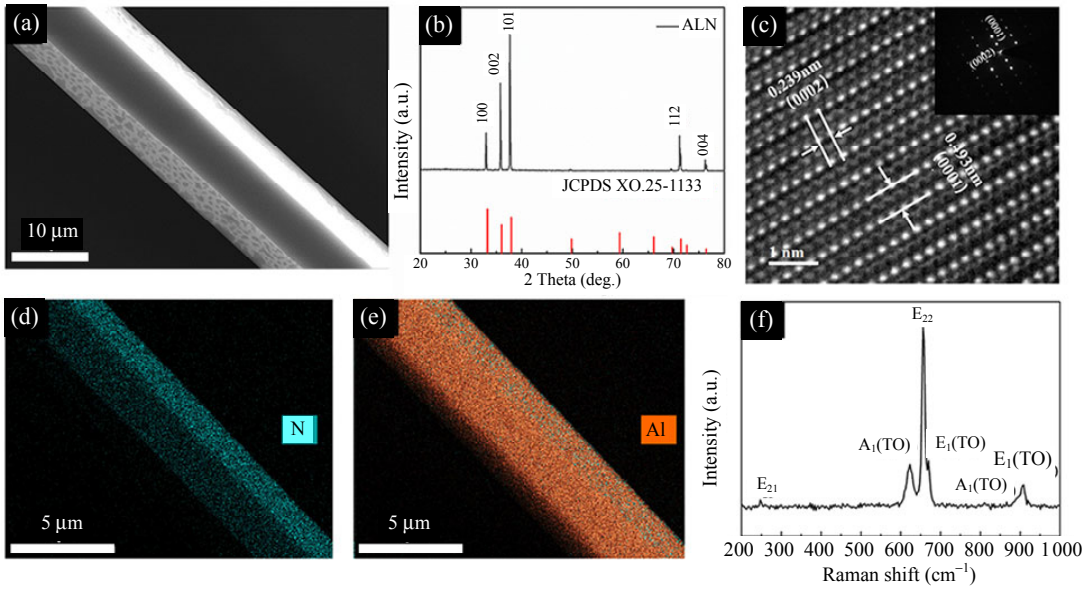

Fig. 1 Morphology and structural characterization of an AlN microwire: (a) typical SEM image of a single AlN microwire, (b) XRD pattern of AlN microwires, (c) TEM image of a single AlN microwir (the upper-right inset provides the SAED pattern), (d) EDX elemental mapping image of N in a single AlN microwire, (e) EDX elemental mapping image of Al in a single AlN microwire, and (f) scattered Raman spectrum of a single AlN microwire, including all Raman phonon modes in the wurtzite AlN structure.

2.2 Operation principle and sensor fabrication

Figure 2(a) shows the schematic diagram of VUV sensing with an optical fiber sensor probe, where the sensor is an AlN microwire based FPI (AlN-FPI) that is integrated in a fiber-tip. Light is delivered by the optical fiber couples into the AlN microwire and reflected back into the fiber by the two end-facets of the microwire, thus forming a fiber-tip FPI. Under VUV illumination, the RI of the AlN microwire changes due to the carrier generation, which will lead to the interference wavelength shift of the AlN-FPI. As illustrated in Fig. 2(b), the preparation of the AlN-FPI fiber probe includes three steps. Firstly, a commercial single-mode fiber (SMF) with a core/cladding diameter of 8.2 μm/125 μm and a length of 1.5 m is fusion spliced to a silica glass tube with an inner/outer diameter of 9 μm/125 μm and a length of about 50 μm at one end, leaving the other end connected to the light source or optical testing system. The fabricated SMF fiber end is placed in the field of view of the microscope of a computer-controlled manipulation system. Then, a single AlN microwire with the proper diameter and length is picked up by the tungsten probe of the manipulation system, both ends of which have been flattened by focused ion beam (FIB) milling to improve the end-face reflectivity and the contact between the microwire and fiber core. Finally, the selected AlN microwire is transferred into the glass tube by carefully moving the tungsten probe of the manipulation system, so that one end of the microwire is tightly attached to the fiber core.

Figure 2(c) shows the experimental setup of VUV sensing for the proposed optical fiber sensor. The device is connected to a super-continuum light source (WhiteLase Micro, NKT Photonics) and an optical spectrum analyzer (OSA, AQ6370C, Yokogawa) through a 3-port optical circulator. Light delivered from the light source is reflected by the AlN-FPI and collected by the OSA, which displays the reflected interference spectrum in real time. The VUV laser beam or pumping light with other wavelengths can be focused onto the sensing probe (namely, AlN-FPI) through a proper lens. The sensitivity can be determined by tracing the interference wavelength shift of the AlN-FPI with the average light intensity increasing.

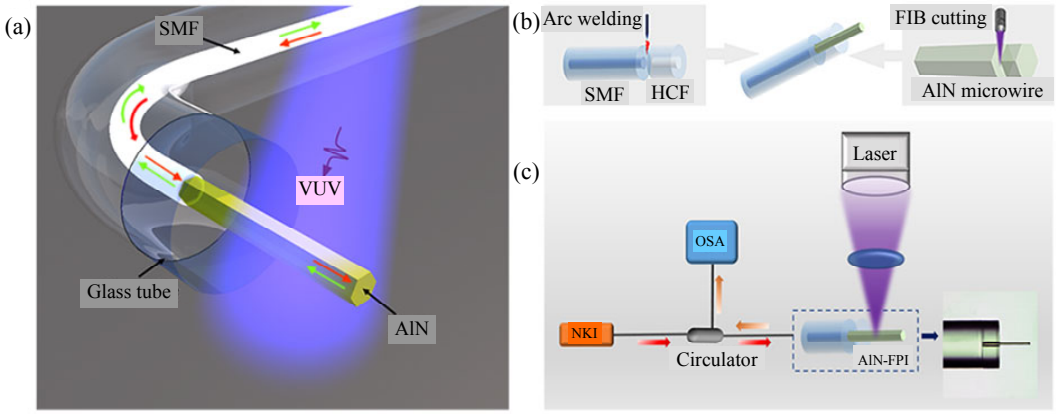

Fig. 2 Illustrations of the device structure, preparation flowchart, and sensitivity test system of the proposed VUV sensor: (a) schematic diagram of the proposed fiber-tip AlN-FPI for VUV sensing, (b) preparation flow chart, and (c) VUV sensitivity measurement system of the fiber-tip AlN-FPI. Note that lasers with the wavelengths of 193 nm, 257 nm, 514 nm, and 908 nm are used here subsequently, and the focusing lens should be replaced accordingly.

3. Results and discussion

Figure 3(a) depicts the reflection spectrum of the proposed fiber-tip AlN-FPI, of which the length L of the AlN microwire is 210 μm, and the free spectral range (FSR) is 2.36 nm around 1 560 nm. The FSR measured from Fig. 3(a) is in good agreement with that obtained from the theoretical estimation, FSR=$\lambda^2/2nL$, where λ is the interference wavelength and n is the RI of the AlN material. The reflection spectrum evolution of the fabricated fiber-tip AlN-FPI under 193 nm VUV irradiation is plotted in Fig. 3(b). As the light intensity gradually increases from 0 W·cm^{-2} to 0.486 W·cm^{-2}, the interference dip at around 1550 nm moves from 1548.64 nm to longer wavelengths, with a total wavelength shift of 1.66 nm. This phenomenon can be attributed to an increase in the RI of the AlN microwire, which is caused by the generation of photocarriers. When the energy of incident photons is higher than the absorption threshold of the AlN semiconductor, valence electrons will transition from the valence band to the conduction band, forming photo-generated electrons and holes. The existence of a large number of photo-generated carriers will cause a detectable change in the absorption coefficient of the material. It can be known from the Kramers-Kronig relationship (K-K relationship) that the change in the absorption coefficient will induce a measurable change of the material RI. The K-K relationship is given by the following formula [25]:

$$\Delta n(N,P,E)=\frac{2c\hbar}{e^2}P\int_0^{\infty}\frac{\Delta\alpha(n,p,E')}{E'^2-E^2}dE' \quad (1)$$

where N and P are the concentrations of free electrons and holes, respectively. The terms $\Delta\alpha$, c, e, E, and $\hbar$ are the changes in the absorption coefficient, the speed of light, the electron charge, the photon energy, and Planck's constant, respectively, and $P\int$ is the principal value integral. Depending on the carrier concentration, there is a competitive relationship between the band-gap filling effect and the band-gap shrinking effect, one of which is dominant and the other is suppressed. For UWBG semiconductors, the band-gap shrinkage effect will dominate the process when the concentration of photocarriers is at a high level. Regarding the band-gap shrinkage, Bennett *et al.* [26] proposed a parabolic model:

$$\Delta\alpha(\chi,E)=\frac{C}{E}\sqrt{E-E_g-\Delta E_g(\chi)}-\frac{C}{E}\sqrt{E-E_g} \quad (2)$$

where χ is the concentration of free electrons or holes, and C is a constant. Since $\Delta E_g(\chi)<0$, $\Delta\alpha$ is always positive. Substituting (2) into (1), one can deduce that Δn is always positive. Therefore, the RI of the AlN microwire increases with the VUV light intensity increasing, resulting in the interference wavelength shift towards longer wavelengths.

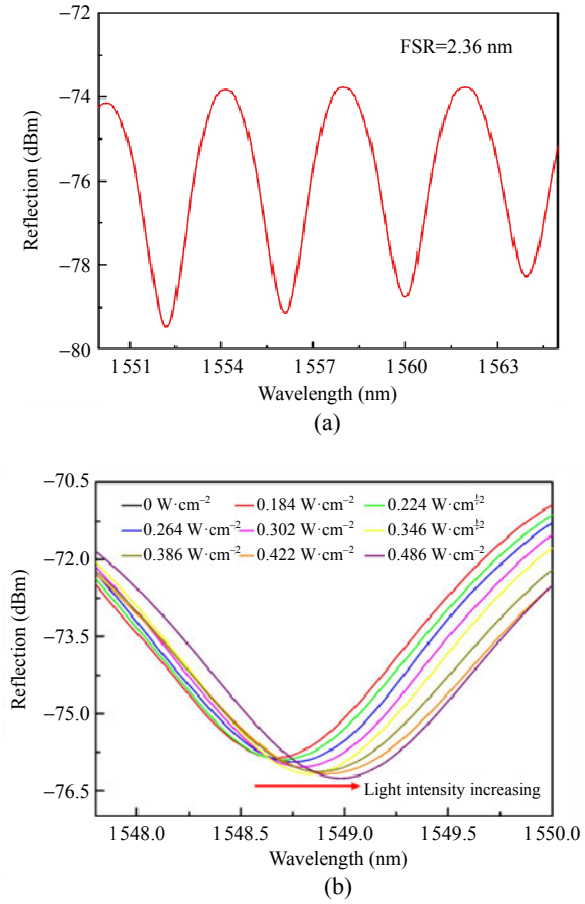

Fig. 3 Reflection spectrum and VUV-induced interference wavelength shift of the proposed sensor: (a) reflection spectrum of a fiber-tip AlN-FPI sensor with a microwire length of 210 μm and an FSR of 2.36 nm and (b) reflection spectrum evolution of the fabricated device under 193 nm VUV light irradiation.

Figure 4 describes the relationship between the interference wavelength and light intensity of the proposed VUV sensor for pump wavelengths at 193 nm, 257 nm, 514 nm, and 980 nm. Under 193 nm VUV illumination, the interference wavelength of the AlN-FPI shifts linearly toward long wavelengths with VUV intensity increasing. The sensitivity can be determined to be 1.03 nm/(W·cm^{-2}) through linear fitting. To verify the wavelength selectivity, the proposed AlN-FPI device is exposed to the irradiation of the solar-blind ultraviolet (SBUV, 257 nm), visible (VIS, 514 nm), and near-infrared (NIR, 980 nm) laser beams, respectively. As can be seen clearly from Fig. 4, the sensitivity drops to 2.07 pm/(W·cm^{-2}) in the case of SBUV irradiation and nearly down to zero in the cases of VIS and NIR irradiation, respectively, which means that the proposed device is only sensitive to VUV. Note that the sensitivity under SBUV irradiation, which is nearly three orders of magnitude lower than that of VUV, is mainly originated from the two-photon absorption (TPA) induced photocarrier generation. This is because the SBUV used here is femtosecond laser pulses, which can provide extremely high peak power to induce TPA processes. Actually, the relationship between the interference wavelength and SBUV intensity is a quadratic function, as shown in the lower inset of Fig. 4, which further proves the existence of the TPA process because the photocarrier density generated through the TPA process is proportional to the square of the incident light intensity. The sensitivity of the proposed sensor under the exposure of 514 nm and 980 nm lasers drops dramatically down to 1.91×10^{-7} nm/(W·cm^{-2}) and 9.87×10^{-6} nm/(W·cm^{-2}), respectively. The insensitivity of the proposed AlN-FPI to VIS and NIR indicates that there is no apparent photothermal effect besides the non-absorption of the AlN microwire in the VIS and NIR bands, meaning that the proposed device indeed does not require extra optical filters.

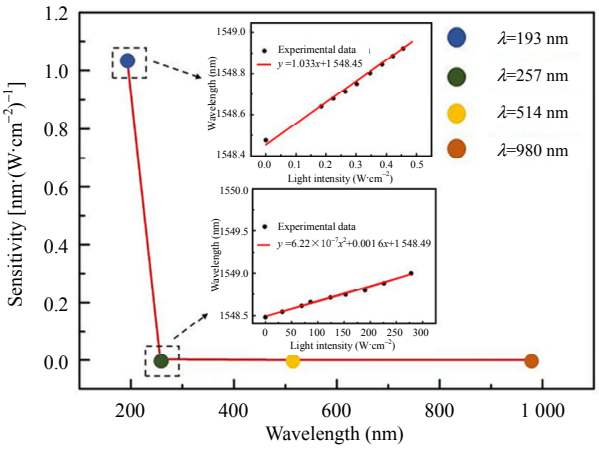

Fig. 4 Relationship between the sensitivity and illumination wavelength for the proposed VUV sensor. Insets show the interference wavelength shift versus light intensities of 193 nm and 257 nm, respectively.

The dynamic response of the proposed VUV sensor is also evaluated according to the edge filtering method with a measurement system as

shown in Fig. 5(a) [27], where the super-continuum light source and OSA in Fig. 2(c) are replaced by a single-frequency tunable laser (Model 81940A, Agilent Technologies) and a photodetector (PD, Model 2053, New Focus) that connect to an oscilloscope (MDO 3054, Tektronix), respectively. The excitation VUV pulses used here are generated from a 50 Hz ArF excimer laser with a central wavelength of 193 nm and a pulse duration of 10 ns, and the on-target light intensity is 0.34 mW·cm^{-2}. The temporal response of the proposed device to 4 laser pulses is depicted in Fig. 5(b), which shows the good stability and fast response. Here, we define the response time of the device to be the duration taken by a signal to change from 10% to 90% between its low and high levels, and vice versa. The magnification of a single-pulse response is shown in Figs. 5(c) and 5(d) to show the rising edge and decay edge, respectively. The rise time (τ_{on}) and decay time (τ_{off}) are measured to be ~10 μs and 0.624 ms, respectively, according to the curves of the rising and decaying edges for 10 successive pulses. Compared with the conventional electric-based VUV photodetectors previously reported, the fiber-optic VUV sensor proposed here exhibits the faster response speed, as listed in Table 1. This is beneficial from the employing of RI changes other than the photocurrent induced by photocarriers in the AlN microwire. The main reason for the slow decay time may possibly originate from the existence of trapped holes (with extended lifetime) and the adsorption of oxygen on AlN surfaces, which may prolong the decay time dramatically [28].

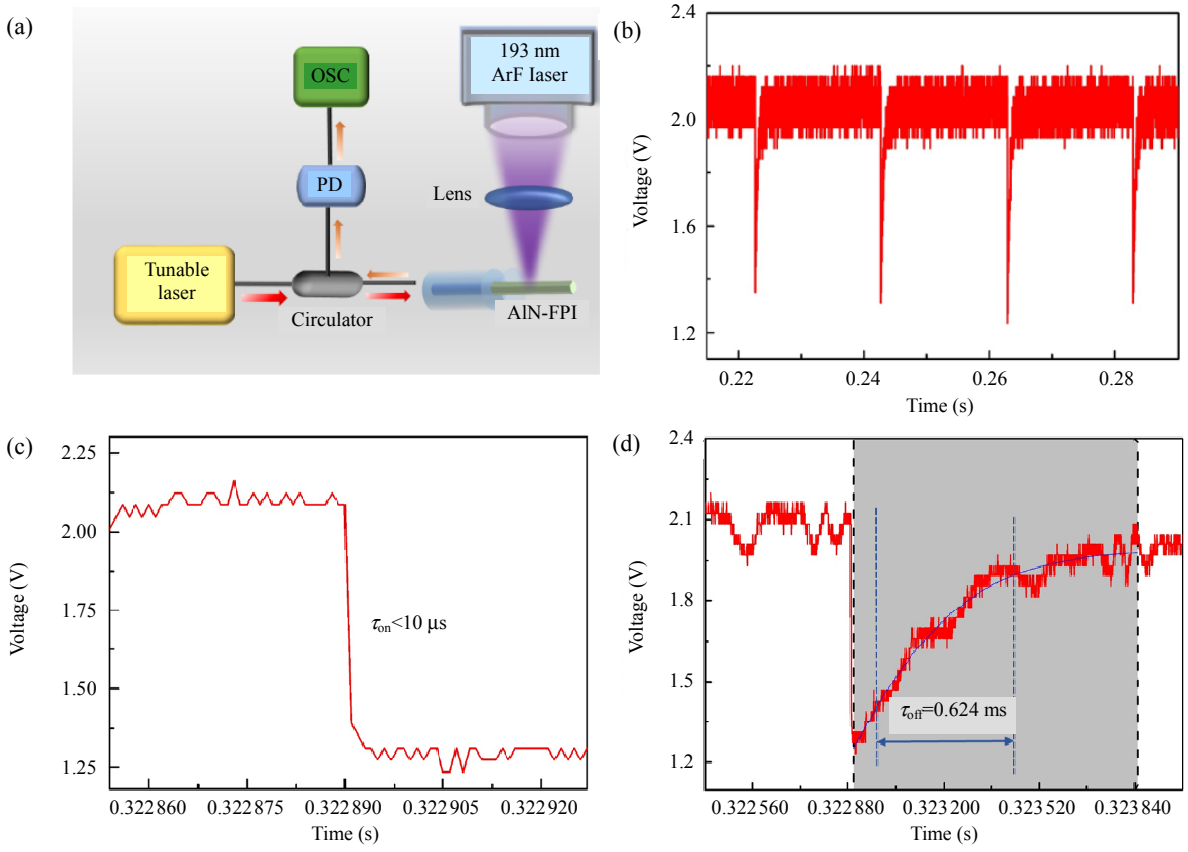

Fig. 5 Temporal response of the proposed VUV sensor: (a) experimental setup for the temporal response measurement of the fiber optic VUV sensor, (b) temporal response of the fiber-tip AlN-FPI under the excitation of 4 successive pulses with a 50 Hz, 193 nm, and 10 ns pulsed VUV laser, (c) magnification of the rising edge, and (d) decaying edge of a single pulse.

Table 1 Comparisons of different typical semiconductor-based VUV photodetectors.

PD	Λ (nm)	Responsivity/sensitivity	τ_{on}	τ_{off}	Ref
p-Gr/AlN/n-ZnO	185	0.04 A·W^{-1}	4.2 μs	1 ms	[29]
AlN micro/nanowire	190	0.39 A·W^{-1}	<0.1 s	<0.2 s	[22]
cBN films	180	0.032 A·W^{-1}	–	–	[30]
AlN film	190	0.004 5 A·W^{-1}	<8 s	<3 s	[31]
p-Gr/AlN/n-GaN	185	0.029 5 A·W^{-1}	2.8 μs	0.77 ms	[23]
Diamond	58.4	–	4 s	–	[32]
MgO	150	1.86 A·W^{-1}	1 s	1 s	[33]
Lamellar AlN	193	5.77 A·W^{-1}	1.8 ms	63.49 ms	[34]
AlN microwire	193	1.03 nm·(W·cm^{-2})$^{-1}$	<10 μs	0.64 ms	This work

4. Conclusions

In summary, a fiber-optic VUV sensor based on an AlN microwire constructed FPI is proposed and demonstrated experimentally. The device shows the excellent performance of VUV sensing with the sensitivity of 1.03 nm/(W·cm^{-2}), rise time of 10 μs, and decay time of 0.64 ms. Compared with the conventional electric VUV detectors, the proposed filterless AlN-FPI device shows the advantages of the fast response, compact size, electromagnetic interference immunity, and radiation resistance in the harsh environment. Benefitting from these features, the proposed sensor is expected to have potential application prospects in the fields of solar physics and space exploration.

Acknowledgment

This work was supported by the National Key Research and Development Program of China (Grant Nos. 2022YFE0111400 and 2022YFB3605303), Science and Technology Innovation Commission of Shenzhen (Grant Nos. JCYJ20200109114001806, JCYJ20220818095615034, and JCYJ20210324095400002), Shenzhen Key Laboratory of Ultrafast Laser Micro/Nano Manufacturing (Grant No. ZDSYS20220606100405013), and Natural Science Foundation of Guangdong Province (Grant No. 2023A1515012893).

Declarations

Conflict of Interest Yiping Wang is an editorial board member for Photonic Sensors and was not involved in the editorial review, or the decision to publish this article. All authors declare that there are no competing interests.

Permissions All the included figures, tables, or text passages that have already been published elsewhere have obtained the permission from the copyright owner(s) for both the print and online format.

References

[1] L. Jia, W. Zheng, and F. Huang. “Vacuum-ultraviolet photodetectors,” *PhotoniX*, 2020, 1(1): 1–25.

[2] D. N. Baker, S. G. Kanekal, X. Li, S. P. Monk, J. Goldstein, and J. L. Burch, “An extreme distortion of the Van Allen belt arising from the ’Hallowe’en’ solar storm in 2003,” *Nature*, 2004, 432(7019): 878–881.

[3] H. V. Cane and I. G. Richardson, “Interplanetary coronal mass ejections in the near-earth solar wind during 1996-2002,” *Journal of Geophysical Research-Space Physics*, 2003, 108(A4).

[4] C. C. Cheng, “The solar wind control of the magnetopause shape: a comparison of a model magnetopause and empirical models,” *Terrestrial Atmospheric and Oceanic Sciences*, 1998, 9(2): 239–254.

[5] M. A. Guerrero and O. De Marco, “Analysis of far-UV data of central stars of planetary nebulae: occurrence and variability of stellar winds,” *Astronomy & Astrophysics*, 2013, 553: A126.

[6] A. Lazarus, J. Kasper, A. Szabo, and K. Ogilvie, “Solar wind streams and their interactions,” *AIP*

Conference Proceedings, 2003, 679(1): 187–189.

[7] D. G. Sibeck, R. E. Lopez, and E. C. Roelof, "Solar wind control of the magnetopause shape, location, and motion," *Journal of Geophysical Research: Space Physics*, 1991, 96(A4): 5489–5495.

[8] D. Basting and G. Marowsky, "*Excimer Laser Technology*," Heidelberg: Springer Berlin, 2005: 86–21.

[9] M. Chini, X. Wang, Y. Cheng, H. Wang, Y. Wu, E. Cunningham, *et al*., "Coherent phase-matched VUV generation by field-controlled bound states," *Nature Photonics*, 2014, 8(6): 437–441.

[10] M. Antonelli, M. Di Fraia, S. Carrato, G. Cautero, R. H. Menk, W. H. Jark, *et al*., "Fast synchrotron and FEL beam monitors based on single-crystal diamond detectors and InGaAs/InAlAs quantum well devices," *Nuclear Instruments & Methods in Physics Research Section A: Accelerators Spectrometers Detectors and Associated Equipment*, 2013, 730: 164–167.

[11] A. BenMoussa, I. E. Dammasch, J. F. Hochedez, U. Schuehle, S. Koller, Y. Stockman, *et al*., "Pre-flight calibration of LYRA, the solar VUV radiometer on board PROBA2," *Astronomy & Astrophysics*, 2009, 508(2): 1085–1094.

[12] M. A. Shea, D. F. Smart, K. G. McCracken, G. A. M. Dreschhoff, and H. E. Spence, "Solar proton events for 450 years: the Carrington event in perspective," *Advances in Space Research*, 2006, 38(2): 232–238.

[13] H. Ishihara, S. Sugio, T. Kanno, M. Matsuoka, and K. Hayashi, "Characterization of photoconductive diamond detectors-candidate vacuum ultraviolet radiation and extreme ultraviolet radiation light source detectors for lithography," *Sensors and Materials*, 2010, 22(7): 357–364.

[14] S. C. Wallace, "Nonlinear optics and laser spectroscopy in the vacuum ultraviolet," *Photophysics and Photochemistry in the Vacuum Ultraviolet. Dordrecht: Springer Netherlands*, 1985: 105–131.

[15] N. De Oliveira, D. Joyeux, and L. Nahon, "Spectroscopy in the vacuum-ultraviolet," *Nature Photonics*, 2011, 5(5): 249–249.

[16] O. Venot, N. Fray, Y. Bénilan, M. C. Gazeau, E. Hebrard, G. Larcher, *et al*., "VUV-absorption cross section of CO_2 at high temperatures and impact on exoplanet atmospheres," in *Colloquium of the CNRS Interdisciplinary Initiative "Planetary Enviroments and Origins of Life*, Paris, France, 2014, pp. 01002.

[17] C. Dujardin, D. Amans, A. Belsky, F. Chaput, G. Ledoux, and A. Pillonnet, "Luminescence and scintillation properties at the nanoscale," *IEEE Transactions on Nuclear Science*, 2010, 57(3): 1348–1354.

[18] B. L. Paredes, H. M. Araújo, F. Froborg, N. Marangou, N. Marangou, T. J. Sumner, *et al*., "Response of photomultiplier tubes to xenon scintillation light," *Astroparticle Physics*, 2018, 102: 56–66.

[19] Hamamatsu Photonics K. K., "*Photomultiplier Tubes: Basics and Applications*," Edition 3a, Hamamatsu: Hamamatsu Photonics, 2007: 38.

[20] M. Richter, A. Gottwald, U. Kroth, A. A. Sorokin, S. V. Bobashev, L. A. Shmaenok, *et al*., "Measurement of gigawatt radiation pulses from a vacuum and extreme ultraviolet free-electron laser," *Applied Physics Letters*, 2003, 83(14): 2970–2972.

[21] A. BenMoussa, A. Soltani, U. Schühle, K. Haenen, Y. M. Chong, W. J. Zhang, *et al*., "Recent developments of wide-bandgap semiconductor based UV sensors," *Diamond and Related Materials*, 2009, 18(5–8): 860–864.

[22] W. Zheng, F. Huang, R. S. Zheng, and H. L. Wu, "Low-dimensional structure vacuum-ultraviolet-sensitive (lambda<200 nm) photodetector with fast-response speed based on high-quality AlN micro/nanowire," *Advanced Materials*, 2015, 27(26): 3921–3927.

[23] T. T. Li, F. Wang, R. C. Lin, W. T. Xie, Y. Q. Li, W. Zheng, *et al*., "In-plane enhanced epitaxy for step-flow AlN yielding a high-performance vacuum-ultraviolet photovoltaic detector," *CrystEngComm*, 2020, 22(4): 654–659.

[24] L. Zhang, Y. Wang, H. Wu, M. X. Hou, J. R. Wang, L. C. Zhang, *et al*., "A ZnO nanowire-based microfiber coupler for all-optical photodetection applications," *Nanoscale*, 2019, 11(17): 8319–8326.

[25] B. R. Bennett, R. A. Soref, and J. A. Del Alamo, "Carrier-induced change in refractive index of InP, GaAs and InGaAsP," *IEEE Journal of Quantum Electronics*, 1990, 26(1): 113–122.

[26] K. F. Berggren and B. E. Sernelius, "Band-gap narrowing in heavily doped many-valley semiconductors," *Physical Review B*, 1981, 24(4): 1971–1986.

[27] C. Liao, D. Wang, Y. Li, T. Sun, and K. T. V. Grattan, "Temporal thermal response of Type II-IR fiber Bragg gratings," *Applied Optics*, 2009, 48(16): 3001–3007.

[28] Y. Liu, C. R. Gorla, S. Liang, N. Emanetoglu, Y. Lu, H. Shen, *et al*., "Ultraviolet detectors based on epitaxial ZnO films grown by MOCVD," *Journal of Electronic Materials*, 2000, 29: 69–74.

[29] W. Zheng, R. Lin, D. Zhang, L. Jia, X. Ji, and F. Huang, "Vacuum-ultraviolet photovoltaic detector with improved response speed and responsivity via heating annihilation trap state mechanism," *Advanced Optical Materials*, 2018, 6(21): 1800697.

[30] A. Soltani, H. A. Barkad, M. Mattalah, B. Benbakhti, J. C. De Jaeger, Y. M. Chong, *et al*., "193 nm deep-ultraviolet solar-blind cubic boron nitride based

photodetectors," *Applied Physics Letters*, 2008, 92(5): 053501.

[31] A. BenMoussa, J. F. Hochedez, R. Dahal, J. Li, J. Y. Lin, H. X. Jiang, *et al*., "Characterization of AlN metal-semiconductor-metal diodes in the spectral range of 44–360 nm: photoemission assessments," *Applied Physics Letters*, 2008, 92(2): 022108.

[32] A. Balducci, M. Marinelli, E. Milani, M. E. Morgada, A. Tucciarone, G. Verona-Rinati, *et al*., "Extreme ultraviolet single-crystal diamond detectors by chemical vapor deposition," *Applied Physics Letters*, 2005, 86(19): 193509.

[33] W. Zheng, R. Lin, Y. Zhu, Z. Zhang, X. Ji, and F. Huang, "Vacuum ultraviolet photodetection in two-dimensional oxides," *ACS Applied Materials & Interfaces*, 2018, 10(24): 20696–20702.

[34] Z. L. Fan, Z. Y. Qin, L. Jin, Z. Y. Yue, B. K. Li, W. F. Zhang, *et al.*, "A solar-blind vacuum-ultraviolet photodetector based won free-standing lamellar aluminum nitride single crystal," *Applied Physics Letters*, 2023, 123(23): 232104.